Accepted Manuscript

Electromagnetic shielding, magnetic and microwave absorbing properties of Polypyrrole/$Ba_{0.6}Sr_{0.4}Fe_{12}O_{19}$ composite synthesized via in-situ polymerization technique

Ninad Velhal, N.D. Patil, Gopal Kulkarni, S.K. Shinde, N.J. Valekar, H.C. Barshilia, Vijaya Puri

PII: S0925-8388(18)34158-6

DOI: https://doi.org/10.1016/j.jallcom.2018.11.041

Reference: JALCOM 48267

To appear in: *Journal of Alloys and Compounds*

Received Date: 20 July 2018

Revised Date: 31 October 2018

Accepted Date: 3 November 2018

Please cite this article as: N. Velhal, N.D. Patil, G. Kulkarni, S.K. Shinde, N.J. Valekar, H.C. Barshilia, V. Puri, Electromagnetic shielding, magnetic and microwave absorbing properties of Polypyrrole/ $Ba_{0.6}Sr_{0.4}Fe_{12}O_{19}$ composite synthesized via in-situ polymerization technique, *Journal of Alloys and Compounds* (2018), doi: https://doi.org/10.1016/j.jallcom.2018.11.041.

Electromagnetic Shielding, Magnetic and Microwave Absorbing Properties of Polypyrrole/$Ba_{0.6}Sr_{0.4}Fe_{12}O_{19}$ Composite Synthesized *via* In-Situ Polymerization Technique

Ninad Velhal[1], N.D. Patil[1], Gopal Kulkarni[1], S. K. Shinde[2], N. J. Valekar[1], H. C. Barshilia[3], Vijaya Puri[1]*

[1]*Thick and Thin Film Device Laboratory, Department of Physics, Shivaji University, Kolhapur, 416004, India*

[2]*Department of Biological and Environmental Science, College of Life Science and Biotechnology, Dongguk University, 410-820, South Korea*

[3]*Surface engineering division, Nanomaterials Research Lab, CS-IR National Aerospace Laboratories, Kodhihalli, Bangalore, 560 017, India*

Email: vijayapuri1@gmail.com

Graphical Abstract:

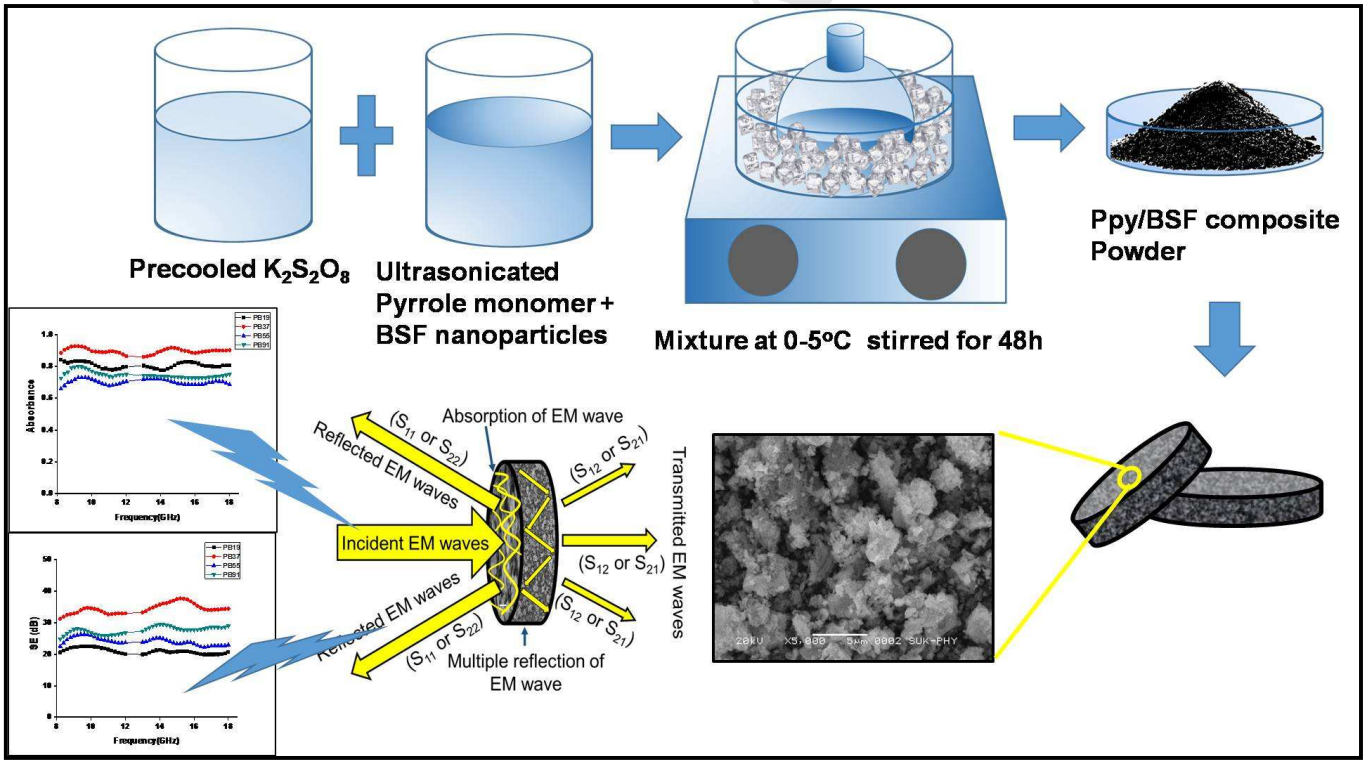

Electromagnetic Shielding, Magnetic and Microwave Absorbing Properties of Polypyrrole/$Ba_{0.6}Sr_{0.4}Fe_{12}O_{19}$ Composite Synthesized *via* In-Situ Polymerization Technique

Ninad Velhal[1], N.D. Patil[1], Gopal Kulkarni[1], S. K. Shinde[2], N. J. Valekar[1], H. C. Barshilia[3], Vijaya Puri[1]*

[1]*Thick and Thin Film Device Laboratory, Department of Physics, Shivaji University, Kolhapur, 416004, India*

[2]*Department of Biological and Environmental Science, College of Life Science and Biotechnology, Dongguk University, 410-820, South Korea*

[3]*Surface engineering division, Nanomaterials Research Lab, CS-IR National Aerospace Laboratories, Kodhihalli, Bangalore, 560 017, India*

Email: vijayapuri1@gmail.com

Abstract

In this article, we have synthesized the Polypyrrole/ $Ba_{0.6}Sr_{0.4}Fe_{12}O_{19}$ (PBSF) composite via in-situ polymerization technique. The synthesized samples were further characterized for structural, electrical, magnetic and microwave absorbing characterizations. The X-ray diffraction patterns reveal the formation of pure hexagonal ferrite phase whereas the Fourier transform infrared spectrums and X-ray photoelectron spectroscopy confirms the formation of polypyrrole/BSF composite structure. The microwave absorbing and shielding properties were studied in the frequency range 8-18 GHz. Using X and Ku band. The magnetic properties were studied using VSM and the PBSF37 composite shows the highest magnetic moment 59.58 emu/gm rather than the other PBSF composites and pure BSF ferrite. The PBSF37 shows the maximum microwave absorption of 89% over the broadband frequency range 8-18 GHz. The maximum shielding effectiveness 37.49 dB at 15.2 GHz corresponding maximum microwave properties were also observed for the same sample.

Keywords: Composite materials; electromagnetic properties; in-situ polymerization; magnetic moment; XPS

Corresponding author

Dr. Vijaya Puri

Email: vijayapuri1@gmail.com

1. Introduction

Recently, conducting polymer composites have received tremendous attention due to their electrical and ferromagnetic properties. Thus the study on this kind of composite materials has become a most active and promising research area [1–3]. Since conducting polymer composites have potential applications in batteries [4], supercapacitors [5], electrochemical display devices [6], molecular electronics [7], electromagnetic shields [8], microwave absorbing materials etc [9]. Now a day's number of communication devices utilizing GHz-range microwave radiation has increased considerably because of their high rate of data transfer. As a consequence, however, electromagnetic interference (EMI) has become a serious issue. So to prevent this problem, microwave absorbers[10] using hexagonal-type ferrite [11,12] or metallic magnetic materials [13–15] or polymeric materials [16–19] are now widely used. So the polymer magnetic composites containing ferromagnetic nanoparticles are studied as promising for different applications [20].

In microwave applications, ferrites serve as better electromagnetic interference (EMI) suppressors than their dielectric counterparts on account of their excellent magnetic properties. Ferrite materials exhibit various electrical and magnetic properties of which complex permeability and complex permittivity, in particular, are important in determining their high-frequency characteristics[21]. Whereas conducting polymers serve as a good electrical conductor with high dielectric loss factor. So the composite these two electric and magnetic component materials play a crucial role in the microwave absorbing material applications. Owing to their advantages in respect to lightweight, low cost, design flexibility, and microwave properties over intrinsic ferrites and polymer [22].

In this paper, we prepared a relatively simple ($B_{0.6}S_{0.4}Fe_{12}O_{19}$)BSF/Ppy nanocomposite to develop a new EM absorbing composite material. BSF nanoparticles were chosen as magnetic components, for their high microwave absorbing properties. While the Ppy was chosen as the electrical component, for its good conductivity and high dielectric loss. BSF/Ppy nanocomposites were prepared via an in-situ oxidation polymerization in an aqueous dispersion of BSF powder. The BSF powder was prepared by a simple auto combustion procedure. The prepared BSF powder was dispersed steadily in a nonpolar phase. However, it was hard for BSF powder to composite with Ppy under this condition due to their poor dispersity in the aqueous phase. Therefore, BSF powder was hydrophilically modified. After hydrophilic

functionalization, the composition of BSF powder with polypyrrole was carried out by the oxidative polymerization of pyrrole in aqueous media. On the basis of some measurements, it is found that this BSF/Ppy nanocomposite has a good electromagnetic wave absorbing performance with a wide frequency range 8-18 GHz.

2. Experimental

2.1 Synthesis of Ppy powder

For the synthesis of polypyrrole powder, the starting materials used were pyrrole monomer, H_2SO_4 and $K_2S_2O_8$. The simple chemical bath deposition technique was used. The detailed procedure of synthesis of Ppy discussed in our previous report[17].

2.2Synthesis of BSF nanoparticles

The starting material was used as $Fe(NO_3)_3 \cdot 9H_2O$,$Sr(NO_3)_2 \cdot 6H_2O$, $Ba(NO_3)_2 \cdot 6H_2O$ and citric acid for the synthesis of BSF nanoparticles. By using the simple and cost effective auto combustion technique the BSF nanoparticles were synthesized. The detailed procedure of the auto combustion technique and the synthesis of BSF powder were discussed in our previous report [23].

2.3 Synthesis of BSF/Ppy nanocomposite

The PPY/BSF composites were synthesized by in situ chemical oxidative polymerization in the presence of optimized BSF nanoparticles, with potassium persulphate ($K_2S_2O_8$) as the oxidant and H_2SO_4as the dopant. A detail preparation process for PPY/BSF composites is as follows: BSF powder was added to 0.1 M H_2SO_4 with DBSA under ultrasonication for 30 min to obtain a uniform suspension, and then the pyrrole monomer was added under ultrasonication for another 30 min to form a pyrrole/ H_2SO_4 mixture containing BSF. In the polymerization reaction the, sulfuric acid plays an important role. Since it produces H^+ ions and SO_4^{--} ions and which takes the part in the polymerization reaction. The mixture was cooled in an ice-water bath for 1 h before a precooled $K_2S_2O_8$ aqueous solution was added for oxidative polymerization for 24 h under vigorous mechanical stirring, with the temperature controlled at 0-5°C. The precipitated powder was centrifuged and washed with distilled water and anhydrous ethanol until the filtrate became colorless and then was dried at 80 °C for 24 h. Throughout the experiment, the molar ratio of pyrrole to H_2SO_4([pyrrole]/[H_2SO_4]) and to $K_2S_2O_8$([pyrrole]/[$K_2S_2O_8$]) was retained at 1:1. The possible reaction mechanism of Ppy/BSF is as follows –

In the polymer reaction, the polymerization technique plays an important role for determining morphology, molecular weight, chain linearity and internal defects in the material. Here we have used the in-situ polymerization technique for the synthesis of polymer ferrite composite. Here the water is the continuous phase whereas the DBSA as a surfactant acts as the discontinuous phase. In typical aqueous solution the dispersed ferrite particles forms the globular or spherical nanoparticles. Generally in emulsion polymerization, there are chances of formation of macroscopic particles and that can be prevented by adding the steric stabilizers like polyvinyl alcohol, poly-(N-vinylpyrrolidone), cellulose ethers, but in this case the DBSA itself acts to prevent the formation of macroscopic precipitations. When monomer solution along with the dopant is added into the ferrite DBSA and into the oxidant solution, the sulphonate ions are formed around the ferrite particles and the polymerization takes place at the interface of boundary. During this reaction the ferrite particles are trapped in polypyrrole porous matrix. The four different mass ratios of the pyrrole monomer to BSF nanoparticles at 1:9, 3:7, 5:5, and 9:1 were prepared respectively. These powders were compressed into small pellets using the hydraulic press. The 10-ton pressure was used for the compression of powder and further these pellets were used for the various characterizations. The schematic of the preparation of Ppy/BSF composite is illustrated in Fig.1.

3. Result and discussion

3.1 X-ray diffraction patterns

The X-ray diffraction patterns of pristine polypyrrole (Ppy), pristine BSF, and Ppy/BSF composites are presented in Fig.2. From fig. it is seen that the peaks observed in pristine BSF are also observed in Ppy/BSF composites. The main peaks of BSF have been observed at 19.08^{o}, 30.52^{o}, 32.30°, 34.32°, 35.74^{o}, 37.29°,40.49°, 42.51°, 50.39^{o}, 54.25^{o}, 55.20°, 56.75°and 63.15°corresponding to the (102), (110), (107), (114), (108), (203), (205), (206), (209) (217), (2011), (220) and (317) reflections, respectively. All the observed peaks were matches with the JCPDS card no.00-051-1879 having an M-type hexagonal crystal structure. This indicates that presence of BSF nanoparticles in the prepared Ppy/BSF composites. The diffraction peaks observed in Ppy/BSF composite diffraction patterns were observed at the same diffraction angle position that of the observed in pristine BSF, this indicates that the structure of BSF was not altered after the in-situ polymerization reaction of Ppy and BSF. With the increase in the content of ferrite nanoparticles in Ppy medium, the intensity of all the diffracted peaks was increased.

This shows that the formation polymer composite having higher crystallinity. On the other hand, the intensity of the all diffracted peaks in the BSF/Ppy composite diffraction patterns were observed to be weak as compared to the intensity of peaks observed in the pristine BSF. This indicates that BSF nanoparticles were get coated with Ppy. From the most intense and prominent peak i.e. (114) the crystallite size for Ppy/BSF nanocomposite particles was calculated. The crystallite size can be calculated by line broadening using Sherrer's formula[24]equation (1)

$$D = \frac{k\lambda}{\beta Cos\theta} \quad \text{---------- (1)}$$

Where λ is the X-ray wavelength,

D is the crystallite size in angstroms,

Θ the Bragg angle in degrees, and

β is the line broadening FWHM measured in radians.

k the shape factor,

The value of k is often assigned as 0.89 which depends on several factors including the Miller index of the reflecting plane and the shape of the crystal.

The average crystallite size for Ppy/BSF nanocomposite has been calculated using the equation (1) and estimated as 48 nm.

3.2 X-ray photoelectron Spectroscopy

X-ray photoelectron spectroscopy (XPS) is a widely used surface analysis technique because it provides valuable quantitative and chemical state information from the surface to a depth of approximately 10 nm. To study the surface components and the valences of the elements of the composite, the samples were further characterized by XPS. The low resolution (survey scan) spectrum of Ppy/ BSF composite consists of 8 peaks: C ls at 284.6 eV, N ls at 399.8, O ls at 532.01 and the oxidation state of iron was inferred from the XPS core-level spectra of Fe 2p. Although a large number of XPS studies approached the iron oxides, to unambiguously discern between them remains a difficult task. According to the wide scan spectra (Fig. 3(a)), Fe peak is not clearly observed and there is a weak peak at 399.8 eV corresponding to the pyrrole nitrogen (-NH-) and the other two peaks of C 1s and O 1s exhibit stronger intensities[25,26]. The C1s core level spectrum (Fig. 3(b)) of the composite mad of three sub peaks at binding energies 284.6, 287.1 and 288.7 eV respectively, which can be attributed to C-C/C-H, C-N and C-O. Also from the wide scan spectra, (Generally in polymers polypyrrole and polyaniline) the N atom of

polypyrrole have three different nitrogen species, namely the imine-like (=N–) with binding energy 398.3 eV, amine-like (–NH–) with binding energy 399.8 eV, and positively charged nitrogen (N+) structure with corresponding binding energy 401.5 eV [26]. This is shown in Fig. 3(c). In addition, The Fe 2p spectrum contains the doublet Fe 2p3/2 and Fe 2p1/2 with binding energy values of 710.49 and 724.06 eV, typical for magnetite (Bhargava et al., 2007). Each peak from Fe 2p spectrum can be deconvoluted into two components corresponding to Fe^{3+} and Fe^{2+} ions from magnetite. One can observe the contribution of the Fe 2p3/2 satellites located at 713.98 eV and 727.17 eV which correspond to Fe^{2+} and Fe^{3+} species (Brundle et al., 1977). The XPS peak of Fe^{2+} is observed at 710.49 eV shown in Fig.3(d), which agrees with the results of previous articles [27,28]. Fig.(e) shows deconvoluted spectrum of O 1s peak of PPy/BSF, in which the peak at 532.01 eV is corresponding to the C–O, C=C and –OH. The deconvoluted spectrum of S2P signal is shown in fig. (f). In which the sulfur located at four places as 163.69, 165.02 and 168.90 which corresponding to Ppy-SO_4 and Ppy-S_2O_8 group [29,30]. This is obtained due to the use of surfactant at the time of reaction. The above mentioned analysis confirms the successful preparation of Ppy/ BSF composite. These results are in also agreement with the XRD data.

3.3 FT-IR Spectroscopy

The FT-IR spectra of the pristine Ppy, BSF and Ppy/BSF composites were recorded using a Perkin Elmer IR spectrophotometer in the range 350-2000cm^{-1} which is depicted in Fig.4. From Fig. it is seen that the Ppy/BSF composite sample contain the characteristic absorption bands of both pristine Ppy and BSF. In ferrites, the metal ions are usually situated in two different sublattices, designated as tetrahedral and octahedral sites according to the geometrical configuration of the oxygen nearest neighbors[9].

In Fig.4 it is seen that the two intense absorption bands observed at ~600 cm^{-1} and ~420 cm^{-1} are of the BSF which are identified as the metal–oxygen stretching vibrations of BSF. The characteristic absorption bands of Ppy occur at 795, 909, 1046, 1094, 1182, 1294, 1479, 1554 and 1706 cm^{-1}. The principal absorption bands observed in the FT-IR spectra of Ppy, with and without BSF are given in Fig.4. From the IR spectrums it is clearly seen that as the Ppy content increases in BSF, the intensity of all the bands which corresponds to Ppy were increased. The peak observed at 1046 cm^{-1} is due to the N-H in-plane deformation, whereas the peak occurred at 908 cm^{-1} is due to the C-H out of plane deformation. The band located at 795 is the C-H out of

plane ring deformation. The band at 1554 cm^{-1} corresponds to the C-C stretching vibrations in pyrrole ring[22, 23].

There are also some bands found in the region from 1250 to 1100 cm^{-1} that correspond to the breathing vibration of the pyrrole ring. The peak of the S=O stretching vibration of sulfonate anion (expected at 1183 cm^{-1} is observed at 1182 cm^{-1}. The band attributed from 1400 to 1250 cm^{-1} is attributed to C–H or C–N in–plane deformation modes and has a maximum at 1294 cm^{-1}. The band at 1479 cm^{-1} is assigned to C–N stretching of the quinoid ring, which arises due to the protonation of Ppy by the dopant [33]. These bands at 1554 and 1479 cm^{-1} are the characteristic bands of the nitrogen benzenoid and quinoid forms and are present due to the conducting state of the polymer. The peaks attributed in the region 800–900 cm^{-1} are the characteristic peaks of para substitution of the aromatic ring and which reveal that the polymerization has proceeded via a head-to-tail mechanism[23–25].A small band observed at 1706 cm^{-1} which correspond to the presence of carbonyl group of prepared polypyrrole composite. From this, it confirms that the Ppy/BSF composite was formed successfully.

3.4 Scanning electron microscopy

The morphology of the obtained Ppy/BSF composite has been studied using scanning electron microscopy. The Fig. 5 shows the scanning electron microscopic images of pristine Ppy, BSF and Pp/BSF composites with different weight ratios. The fig. 5 (a) shows the pristine Ppy. It indicates that the Ppy nanoparticles have uniformly distributed. After the 10weight percent mixing of BSF nanoparticles in the Ppy nanoparticles medium (PBSF91) there is no drastic change in morphology was observed but at the 50 weight percent mixing of BSF nanoparticles in Ppy medium the good dispersion of BSF nanoparticles were observed. Also, the slight agglomeration was started. After 70 weight percent mixing the strong agglomeration between Ppy and BSF nanoparticles were observed and the bunches of Ppy/BSF nanocomposite were formed. In 70-30% nanocomposite sample, Ppy has enwrapped the BSF nanoparticles effectively, and composite particles are irregular in shape with a rough surface which creates the bunches of composite nanoparticles. Further increasing the concentration of BSF nanoparticles at PBSF19 (e), it indicates the non- uniform distribution of composite nanoparticles.

3.5 DC electrical conductivity

The room temperature electrical resistance of Ppy, BSF and Ppy/BSF composite pellets was measured using two-point probe method.

The resistivity and DC conductivity were calculated using the equation (2)

$$\rho = \frac{RA}{l} \quad \text{---------- (2)}$$

Where R is the resistance of the film

A is the area of the film

L is the length of the film

Table 1 depicts the variation of resistance with Ppy/BSF ratio. From this table, it is observed that the pristine Ppy shows the maximum conductivity of 49.70 $x10^{-3}$ S/cm while the pure BSF pellet shows the maximum resistivity. As ferrite content increases from 10-90% in the Ppy the resistivity increases and conductivity decrease from 0.0484 x 10^{-6} to 49.70 $x10^{-3}$ The increasing resistance of nanocomposite may be attributed to the insulating and magnetic behavior of the BSF nanoparticles which acts as core and partial blockage of the conductive path also resistance increased by increasing M_s of nanoparticles. Also, there were so many factors for interpreting conductivity such as a dopant, doping level, crystallinity, the length of conjugate chain, the interaction between conjugate chains, and molecular weight, etc. It was known that the Ppy was a conducting polymer while the ferrite particles were insulators, so the conductivity of the composites may decrease with the ferrite content. The introduction of the ferrite particles would affect the crystallinity of the Ppy, further resulted in destroying the conjugated degree, continuity, and regularity of the chains. Besides, the interaction between the ferrite particles and Ppy chain, and possible bonding effect between the metal cation and the Ppy made the electronic density of the polymer chain reduce and hence resulted in the decrease of the conductivity [36–38].

3.6 Magnetic Properties

Magnetic properties of pure Ppy, BSF and its composite with Ppy were studied using Vibrating Sample Magnetometer (VSM).Fig.6 depicts the magnetization (M) versus applied field (H) for pure BSF and Ppy/BSF composites with a different weight ratio of polymer with BSF. The magnetic properties of BSF and Ppy/BSF composites were analyzed at room temperature with an applied field $-10kOe \leq H \leq 10kOe$.

The magnetic parameters such as coercivity (H_c), saturation magnetization (M_s), remanence (M_r) and squareness of the loop (M_r/M_s) calculated from hysteresis loops for Ppy, BSF and different composites of Ppy/BSF were tabulated in Table 1. The BSF and all

composites of Ppy/BSF show the ferromagnetic behavior and magnetically they are hard at room temperature. The single-phase-like smooth hysteresis loops implying that the existence of the exchange coupling phenomena in the Ppy/BSF composite[27,28].The value of saturation magnetization and coercivity of pure BSF is as expected high i.e. 95.59 emu/gm and 3812 Oe respectively. In the case of Ppy/BSF composites, as the BSF content increases in the Ppy medium the value of M_s, M_r and H_c increases as expected up to 30-70% ratio of Ppy to BSF. The M_s, M_r and H_c vary from 37.31 to 59.85emu/gm, 22.97 to 33.16emu/gm and 3400 to 4487 Oe respectively. The increase in saturation magnetization is due to the high polydispersivity of the BSF in Ppy matrix that arises due to the functionalization of nano ferrites particles with the surfactant DBSA and also the BSF have ferromagnetic nature[22][41]. After the 30-70% at 10-90% the value of all M_s, M_r and H_c were drastically decreased and it was observed to be 49.72 emu/gm, 30.11 emu/gm and 3419 Oe respectively. Magnetization and coercivity exhibit monotonous increasing functions with the content of BSF nanoparticles in Ppy/BSF nanocomposite. After the weight ratio increased up to 30-70%, the dipolar interaction is suppressed by the exchange-coupling interaction and it will dominate in nanocomposite ferrite systems. The increase of effective anisotropy will result in a decrease in exchange length L_{ex} according to eq. (3)

$$L_{ex} = \left(\frac{A}{< K >} \right)^{1/2} \text{---------- (3)}$$

Where A is exchange stiffness constant

⟨K⟩ is the effective anisotropy and

L_{ex} is the exchange length

The exchange-coupling interaction deteriorates, which leads to the coercivity reduction. Therefore, the H_c value is lower than 10-90% K and its difference has achieved a maximum value for the nanocomposite with a mass ratio of 30-70%, which implies that the hard BSF and nonmagnetic Ppy grains are sufficiently exchange-coupled. Also when the metal cations at the surface layer of nanoparticles are coordinated with ligands, the spin-orbital coupling is reduced, and consequently the surface anisotropy decrease, which causes the reduction of the coercivity of composites [42,43].

In polymer ferrite nanocomposite the magnetic properties strongly depend on magnetite or ferrite particles that have been believed to be highly dependent on the highly dependent on the sample shape, crystallinity, and the value of magnetic particles, so that they can be adjusted to obtain optimum property[9].The squareness ratio of the BSF and its composite with Ppy lies in between 0.5 to 0.6 and which reveals the Ppy/BSF nanocomposite exhibit the single magnetic domain characteristic. Usually, the lower values are associated with larger particles and domain-wall formation, and higher values with texture [44].

According to Stoner-Wolfarth [45] theory the coercivity, H_c, of nanoparticles is determined by magnetocrystalline anisotropy constant K and saturation magnetization M_s (eq. 4)

$$H_c = \frac{2K}{\mu_o M_s} \quad \text{---------- (4)}$$

Where μ_o is the universal constant of permeability in free space, $4\pi \times 10^{-7}$H/m. Thus, K can be calculated combining the product of H_c and M_s, and it can be easily deduced that the value of K is also a monotone increasing function with the content of BSF nanoparticles in Ppy/BSF nanocomposites, that is, the more Ppy coating on the BSF nanoparticles produces samples with smaller K. In M-type barium ferrites, lowering the anisotropy field results in lower natural resonance frequency. Because the observed magnetic properties of nanoparticles area combination of many anisotropy mechanisms, the Ppy coating on the BSF nanoparticles will likely affect the contributions of the surface anisotropy, shape anisotropy, and interface anisotropy to the net anisotropy, K. Therefore, in polymerization of pyrrole with BSF nanoparticles, hard magnetic materials with alternative conductivities and magnetic properties can be produced [46,47].

4. Microwave properties

4.1 Transmittance and reflectance

The fig.7 depicts the transmittance and reflectance versus frequency of pristine Ppy, BSF and Ppy/BSF composites with different weight ratios. From fig.6 it is clear that as the ferrite content increases in the polymer, the transmittance of the composite decreases and the PBSF37 composite shows the minimum transmittance. The average transmittance of the composite is about 2.9 % in the 8-18 GHz frequency range. Whereas in the case of reflectance, with an increase in ferrite content reflectance increases and the PBSF55 shows the highest reflectance

and the average reflectance of PBSF55 is about 20%. This may be due to the morphology of composite. Since the polypyrrole has a globular morphology and the BSF have nanoparticles with spherical morphology. The interconnected nano globule was combining with the BSF nanoparticles and forms the denser morphology. This results into the decrease in transmittance of the PBSF37 composite[48]. On the other hand, the magnetic nanoparticles of the ferrite are more responsible for increasing the reflectance of that composite. The PBSF37 composite shows the lower transmittance and lower reflectance than the other composites.

4.2 Microwave absorbance

The plot of absorbance versus frequency present in the Fig.8 The absorbance of the composite was calculated from the data of transmittance and reflectance using the eq. (5)

$$A = 1 - T - R \text{ or } A = (1 - T - R)x100 \text{ ---------- (5)}$$

In conductive materials, absorption can also arise from resistive losses which consist in transforming the electromagnetic energy in heat by Joule effect [49]. It is seen from fig. the absorbance of the composite varies with the frequency and it varies irregularly with the ferrite or polymer content. The PBSF55 shows the minimum absorption 70% whereas the PBSF37 composite shows the highest absorbance 89% which is high as compared to the other composite. Since it can be seen from the data of transmittance and reflectance the composite PBSF37 shows the minimum transmittance and minimum reflectance and hence the absorbance of the PBSF37 composite increases. Also, the surface of the PBSF37 is compact and dense which is also responsible for the increase in absorbance of the composite since the denser morphology is more suitable for the microwave absorption. In the composite PBSF37 the Ppy and BSF are formed the strongly interconnected network of the cauliflower and magnetic nanoparticles and which will increase the resultant absorption of the material.

4.3 Shielding effectiveness (S.E.)

Electromagnetic shielding effectiveness is described as the attenuation of electromagnetic radiation by reflection or absorption in a material. In polymer composites, shielding mechanisms are more complicated than those for homogeneous conductive materials because of the huge surface area available for reflection and multiple-refection. The first reflection of an EM wave from a conductive material surface should be distinguished from the multiple reflectionmechanisms which is the re-reflection of the waves already reflected [50]. The plane

wave shielding theory developed by Schelkunoff[12] and Schultz et al.[51] defines the shielding effectiveness SE as- eq. (6)

$$SE = A + R + B \quad \text{---------- (6)}$$

Where B is a term which takes into account the loss caused by multiplereflections inside the shield, R is the reflection loss, and A is the absorption loss.

The EMI shielding effectiveness (SE) of a material is defined as the ratio of transmitted power to incident power. Fig.9 shows the variation of SE with frequency in the frequency range 8-18GHz. The SE of the composite varies from 20.40 dB 37.49 dB. The minimum shielding effectiveness is observed 20.40 dB at 8.2 GHz while the maximum shielding effectiveness observed 37.49 at 15.2 GHz. From fig. it also observed that as the ferrite content increases the polymer the SE decreases continuously but at composite PBSF37 it shows the maximum value. The SE of materials depends on the level of the conductivity and permittivity of the materials and their variation with frequency. This may be due to that, at certain level or at particular composition (PBSF37) the total internal reflections in the materials get increased and these increased internal reflections were attenuate the microwave radiation or which will compel to absorb the microwave radiations and hence the SE of the material increases , which results into the increase in absorption.

4.4 Real and imaginary part of complex permittivity

The VSWR slotted section was used to measure the permittivity of the sample. From the position of minima and from the reflection coefficient the complex permittivity was calculated using the Chapman [52] eq.(7)

$$\varepsilon' = \left(1 + \frac{\Delta\phi\lambda o}{360d}\right) \text{and} \; \varepsilon'' = \left(\frac{\Delta\phi\lambda o\sqrt{\varepsilon'}}{8.686\pi d}\right) \quad \text{---------- (7)}$$

Where $\Delta\phi$ is the difference of the phase shift with and without sample

λo is the wavelength of the corresponding frequency and

d is the thickness of the sample

The plot of real and imaginary part of permittivity versus frequency is presented in fig.9. It is seen from the real and imaginary part both decreases with the frequency. This may be due to the different polarizations occurred in the polymer ferrite composite.

In polypyrrole strong polarization occurs due to the presence of polaron/bipolaron and other bound charges, which leads to a high value of ε’ and ε”. As frequency increases the dipole

present in the system cannot reorient themselves along with the applied electric field, as a result, dielectric constant decreases. It is observed from graph also. The real part of permittivity varies from 59.40 at 8.2GHz to 7.60 at 18 GHz whereas the imaginary part varies from 41.57 at 8.2 GHz to 2.08 at 18 GHz. In a complex hexagonal structure of hexaferrites, positive and negative ions of different valences are separated at the varying bond lengths it generates different strengths dielectric moments which give rise to dipolar polarization. Also, in polycrystalline ferrites, low resistive grains are separated by highly resistive grain boundary, which creates heterogeneity and it gives the interfacial polarization. Both the phenomena contribute to the dielectric constant (ε'). The dielectric loss (ε") in the ferrites, however, depends on the number and nature of the different ions present to exhibit relaxation behavior. The presence of ferrous Fe^{2+} ion and ferric Fe^{3+} ion in ferrites also contributes to the values of ε' and ε" due to enhanced conduction and electron hopping mechanisms[53]. Moreover, when the frequency of electron hopping between Fe^{3+} to Fe^{2+} ions matches that of the microwave, a dielectric resonance phenomenon occurs, which is responsible for the high dielectric loss[54]. In present ferrite–polymer composite, the contribution to dielectric constant and dielectric loss also occur due to interfacial polarization and its relaxation as the semiconducting ferrite particles separated by insulating matrix molecules giving rise to heterogeneity. Different relaxation frequencies of various dipoles formed in the ferrite structure, hopping of electrons and the relaxation due to interfacial polarization all are responsible for the oscillatory behavior of absorption in the samples. However, as the ferrite content in the composite is increased high and smooth loss curves are obtained[54]. This can be attributed to the overlapping of individual relaxation peaks of different dipoles and dominance of relaxation due to interfacial polarization [55].

In polypyrrole composite both the phenomenon's happen together hence resulting in high SE value. The polypyrrole composite PBSF37 has lower dielectric constant but the higher dielectric loss which corresponds to enhanced value of SE due to absorption [22].

4.5 Microwave conductivity

The microwave conductivity is directly related to the imaginary part of permittivity so the microwave conductivity of the Ppy/BSF composite can be calculated using the eq. (8).

$$\sigma = 2\pi f \varepsilon o \varepsilon'' \text{ ---------- (8)}$$

The graph of microwave conductivity versus frequency is shown in fig.11. From the graph of microwave conductivity, it is seen that microwave conductivity increases with frequency. The

microwave conductivity varies between 2.09-27.84. The increase in the content of ferrite in composite increases the interaction of electrons with lattice ions through long-range forces and the resulting interaction produces lattice polarization, which acts as a potential well. This hinders the movement of an electron and, hence, decreases the mobility of the material. This indicates the loss of polaron type of conduction, which supports the dielectric loss in microwave region[41].The PBSF37 composite shows the highest value of microwave conductivity and which support to the high microwave absorption.

Here the microwave conductivity is larger than DC conductivity of the composite. This is may be due to low protonation. This supports a metallic island model for conduction with a combination of hopping and electronic conduction occurring depending on dopant level. For higher protonation levels, microwave conductivity approaches the DC conductivity at room temperature[56]. As seen from the graph of transmittance and reflectance, the transmittance shows much lower value than the reflectance and also the microwave conductivity is quite high. There might be a collapse of electric field component of the microwave radiation occurring when it impinges on the high conductivity film. The composite materials are very promising materials for their microwave applications. Since those materials exhibit good complementarities between dielectric loss and magnetic loss, the microwave absorbing properties are closely related to the structure.

5. Conclusion

The Ppy/BSF nanocomposites were successfully synthesized via in-situ polymerization technique. XRD patterns and XPS study shows the formation of BSF/Ppy composite with intense peaks of BSF ferrites. With increasing polymer content in ferrite, the intensity of diffraction peaks decreases. In FT-IR spectrum, the peaks present at ~400 cm^{-1} and ~600 cm^{-1} in the ferrite sample are also observed in the BSF/Ppy composite sample which confirms the formation of BSF/Ppy composite. The surface morphology of BSF/Ppy sample shows the porous structure with increasing polymer content in the ferrite sample and the grain boundaries are clearer at 30-70% composite sample. The magnetic study reveals the highest saturation magnetization (59.85emu/g) and coercivity (33.02emu/gm) was observed at 30-70% composite sample. While the squareness ratio of 30-70% sample shows the 0.55 which confirms Ppy/BSF nanocomposite exhibits the single magnetic domain characteristic. The 30-70% composite sample shows the minimum transmittance and higher reflectance in the whole X and Ku-band frequency range.

The 30-70% composite shows the good SE value (37.49 dB) with high microwave absorption about 89%. The real and imaginary part of permittivity decreases with increase in frequency and the microwave conductivity is much greater than the DC conductivity.

6. Acknowledgement

One of the author Dr. Vijaya Puri gratefully acknowledges UGC India for Award of Research Scientist 'C'. The authors also thank UGC-SAP and DST-FIST for their assistance. All authors thanks, PIFC, Department of Physics, SUK for providing instrumentation facility.

References

[1] M. Kryszewski, J. Jeszka, Synth. Met. 94 (1998) 99–104.

[2] H. Nguyen Cong, K. El Abbassi, J.L. Gautier, P. Chartier, Electrochim. Acta 50 (2005) 1369–1376.

[3] A. Chen, H. Wang, B. Zhao, X. Li, Synth. Met. 139 (2003) 411–415.

[4] H. Nguyen-Cong, V. De la Garza Guadarrama, J.L. Gautier, P. Chartier, Electrochim. Acta 48 (2003) 2389–2395.

[5] P. Bhattacharya, S. Dhibar, G. Hatui, A. Mandal, T. Das, C.K. Das, RSC Adv. 4 (2014) 17039.

[6] S.H. Talale, A Lee, J Y Jang, J Choo, D J Park, G. Huh, J.A. Romagnoli, IEEE (1999) 947–951.

[7] K.S. Jang, H. Lee, B. Moon, Synth. Met. 143 (2004) 289–294.

[8] D.A. Makeiff, T. Huber, Synth. Met. 156 (2006) 497–505.

[9] S.H. Hosseini, A. Asadnia, J. Nanomater. 2012 (2012) 1–6.

[10] K. Shimba, K. Furuta, N. Morimoto, N. Tezuka, S. Sugimoto, Mater. Trans. 52 (2011) 740–745.

[11] D.C. Kulkarni, V. Puri, Microelectron. Int. 27 (2010) 143–147.

[12] B. Mušič, M. Drofenik, P. Venturini, A. Žnidaršič, Ceram. Int. 38 (2012) 2693–2699.

[13] Y. Li, Y. Huang, S. Qi, L. Niu, Y. Zhang, Y. Wu, Appl. Surf. Sci. 258 (2012) 3659–3666.

[14] S. Tyagi, P. Verma, H.B. Baskey, R.C. Agarwala, V. Agarwala, T.C. Shami, Ceram. Int. 38 (2012) 4561–4571.

[15] T.H. Ting, Y.N. Jau, R.P. Yu, Appl. Surf. Sci. 258 (2012) 3184–3190.

[16] N. Velhal, N. Patil, S. Jamdade, V. Puri, Appl. Surf. Sci. 307 (2014) 129–135.

[17] N.B. Velhal, N.D. Patil, V.R. Puri, J. Electron. Mater. 44 (2015) 4669–4675.

[18] S. Jamadade, S. Jadhav, V. Puri, Sch. Reeasrch Libr. 1 (2010) 205–210.

[19] N. Velhal, G. Kulkarni, N.D. Patil, V. Puri, Mater. Res. Express 5 (2018) 106407.

[20] N. Svetoslav, K Tatyana, K Andrey, Y Chavdar, G Ivan, J. Nanosci. Nanotechnol. 8 (2008) 650–654.

[21] H. Bayrakdar, Prog. Electromagn. Res. M 25 (2012) 269–281.

[22] A. Ohlan, K. Singh, A. Chandra, S.K. Dhawan, Appl. Phys. Lett. 93 (2008) 053114.

[23] N. Velhal, G. Kulkarni, D. Mahadik, P. Chowdhury, H. Barshilia, V. Puri, J. Alloys Compd. 682 (2016) 730–737.

[24] N.B. Velhal, N.D. Patil, A.R. Shelke, N.G. Deshpande, V.R. Puri, AIP Adv. 5 (2015) 097166.

[25] R. Turcu, D. Bica, L. Vekas, N. Aldea, D. Macovei, A. Nan, O. Pana, O. Marinica, R. Grecu, Rom. Reports Phys. 58 (2006) 359–367.

[26] M. Qiao, X. Lei, Y. Ma, L. Tian, K. Su, Q. Zhang, Ind. Eng. Chem. Res. 55 (2016) 6263–

6275.

[27] A. Nan, I. Craciunescu, R. Turcu, Asp. Fundam. Appl. Conduct. Polym. (2009) 159–182.

[28] C. Chen, W. Fu, Q. Zhou, J. Wuhan Univ. Technol. Mater. Sci. Ed. 28 (2013) 990–996.

[29] J. Tabačiarová, M. Mičušík, P. Fedorko, M. Omastová, Polym. Degrad. Stab. 120 (2015) 392–401.

[30] K. Idla, A. Talo, H.E.M. Niemi, O. Forsén, S. Yläsaari, Surf. Interface Anal. 25 (1997) 837–854.

[31] H. Eisazadeh, World J. Chem. 2 (2007) 67–74.

[32] M. Omastová, M. Trchová, J. Kovářová, J. Stejskal, Synth. Met. 138 (2003) 447–455.

[33] O. Yavuz, M.K. Ram, M. Aldissi, P. Poddar, S. Hariharan, J. Mater. Chem. 15 (2005) 810–817.

[34] M.J. Gonzalez-Tejera, M.A.D. La Plaza, E. Sanchez de la Blanca, I. Hernandez-Fuentes, Polym. Int. 31 (1993) 45–50.

[35] H.N.M.E. Mahmud, A. Kassim, Z. Zainal, W.M.M. Yunus, J. Appl. Polym. Sci. 100 (2006) 4107–4113.

[36] R. Kostić, D. Raković, S.A. Stepanyan, I.E. Davidova, L.A. Gribov, J. Chem. Phys 102 (1995) 3104–3109.

[37] A. Elahi, N.A. Niaz, M.S. Awan, A. Shakoor, K. Mahmood, Y. Khan, Polym. Sci. Ser. B 57 (2015) 738–749.

[38] W. Chen, X. Li, G. Xue, Z. Wang, W. Zou, Appl. Surf. Sci. 218 (2003) 215–221.

[39] M.K. Ray, K. Bagani, S. Banerjee, J. Alloys Compd. 600 (2014) 55–59.

[40] H. Yang, M. Liu, Y. Lin, Y. Yang, J. Alloys Compd. 631 (2015) 335–339.

[41] N. Patil, N.B. Velhal, R. Pawar, V. Puri, Microelectron. Int. 32 (2015) 25–31.

[42] X. Shen, F. Song, J. Xiang, M. Liu, Y. Zhu, Y. Wang, J. Am. Ceram. Soc. 95 (2012) 3863–3870.

[43] Y. Zhang, Z. Huang, F. Tang, J. Ren, Thin Solid Films 515 (2006) 2555–2561.

[44] C. Tauxe, L Neal Bertram, H Seberino, Geochemistry Geophys. Geosystems 3 (2002) 1–22.

[45] E.P. Stoner, E C Wohlfarth, R. Soc. London. Ser. A, Math. Phys. Sci. 240 (1948) 826.

[46] P. Xu, X.J. Han, J.J. Jiang, X.H. Wang, X.D. Li, a H. Wen, J. Phys. Chem. C 111 (2007) 12603–12608.

[47] N.D. Patil, N.B. Velhal, N.L. Tarwar, V.R. Puri, Int. J. Eng. Innov. Technol. 3 (2014) 73–77.

[48] P. Xu, X. Han, C. Wang, H. Zhao, J. Wang, X. Wang, B. Zhang, J. Phys. Chem. B 112 (2008) 2775–2781.

[49] I. Morari, C. Balan, I. Pintea, J. E. Chitanu, E. Iordache, Prog. Electromagn. Res. M 21 (2011) 93–104.

[50] M.H. Al-Saleh, U. Sundararaj, Carbon N. Y. 47 (2009) 1738–1746.

[51] R.B. Schulz, V.C. Plantz, D.R. Brush, IEEE Trans. Electromagn. Compat. 30 (1988) 187–201.

[52] P B Kashid, Ninad Velhal, Gopal Kulkarni, Priyanka Kandesar, D. V. Ruikar, Vijaya Puri, J. Mater. Sci. Mater. Electron. 29 (2018) 1748–1758.

[53] Z. Haijun, L. Zhichao, M. Chenliang, Y. Xi, Z. Liangying, W. Mingzhong, Mater. Chem. Phys. 80 (2003) 129–134.

[54] S.M. Abbas, R. Chatterjee, A.K. Dixit, A.V.R. Kumar, T.C. Goel, J. Appl. Phys. 101 (2007) 74105–74106.

[55] S.M. Abbas, A.K. Dixit, R. Chatterjee, T.C. Goel, J. Magn. Magn. Mater. 309 (2007) 20–24.

[56] H. H. S. Javedi and K. R. cromack, Phys. Rev. B 39 (1989) 3579–3584.

Table Captions:

Table 1 Resistivity and conductivity of pristine Ppy, pristine BSF, Ppy/BSF composite pellets with different mass ratios

Table 2 Variation of M_s, M_r, H_c and squareness ratio with Ppy to BSF ratio

Table 1

Samples	Resistivity (Ω cm)	Conductivity (S/cm)
BSF	20.63×10^{6}	0.0484×10^{-6}
PBSF19	9.45×10^{5}	0.1058×10^{-5}
PBSF37	10.3×10^{5}	0.0970×10^{-5}
PBSF55	8.21×10^{5}	0.1218×10^{-5}
PBSF91	5.65×10^{4}	0.1769×10^{-4}
Ppy	2012×10^{3}	49.70×10^{-3}

Table 2

Sample	M_s (emu/gm)	M_r (emu/gm)	H_c (Oe)	M_r/M_s
Ppy	0.018	0.011	3705	0.61
PBSF19	49.72	30.11	3414	0.60
PBSF37	59.85	33.02	4494	0.55
PBSF55	53.49	32.61	4368	0.60
PBSF91	37.49	22.97	3653	0.61
BSF	95.59	56.92	3818	0.59

Figure Captions:

Fig. 1 Schematic of preparation of Ppy/BSF composite

Fig. 2 X-ray diffraction patterns of pristine Ppy, BSF and Ppy/BSF composites.

Fig. 3 XPS Spectrum (a) Wide survey scan spectra of PBSF (b) and decovoluted (c), (d), (e) and (f) XPS spectra of PBSF

Fig. 4 FT-IR spectra of pristine Ppy, BSF and Ppy/BSF composite

Fig. 5 SEM images of pristine Ppy, BSF and Ppy/BSF composites with different weight ratios of Ppy to BSF

Fig. 6 Magnetic hysteresis loops of pure BSF and Ppy/BSF composites

Fig. 7(a) Transmittance and **(b)** reflectance of Ppy thin films with different oxidants

Fig. 8 Microwave Absorbance of Ppy/BSF composite

Fig. 9 Shielding effectiveness of Ppy/BSF composites

Fig. 10(a) Real and **(b)** imaginary part of complex permittivity of Ppy/BSF composite

Fig. 11 Microwave conductivity of Ppy/BSF composite

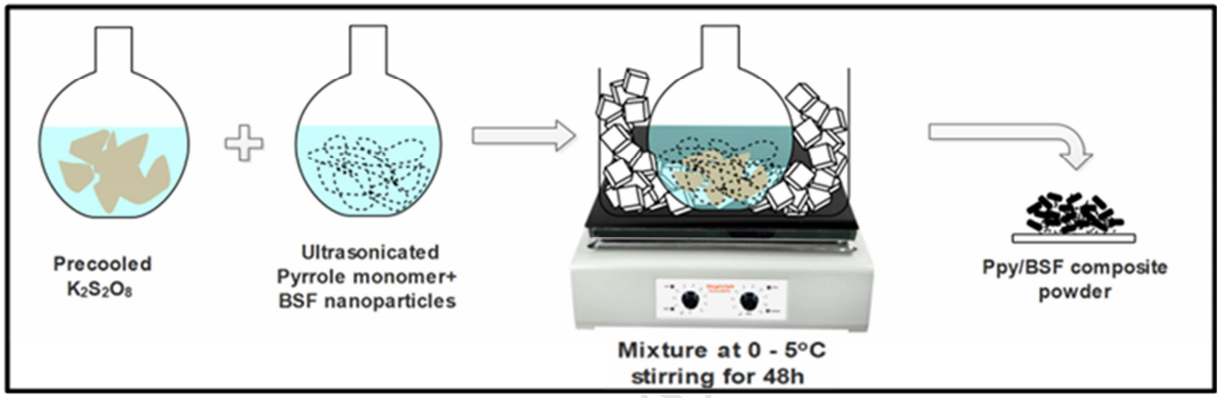

Fig. 1

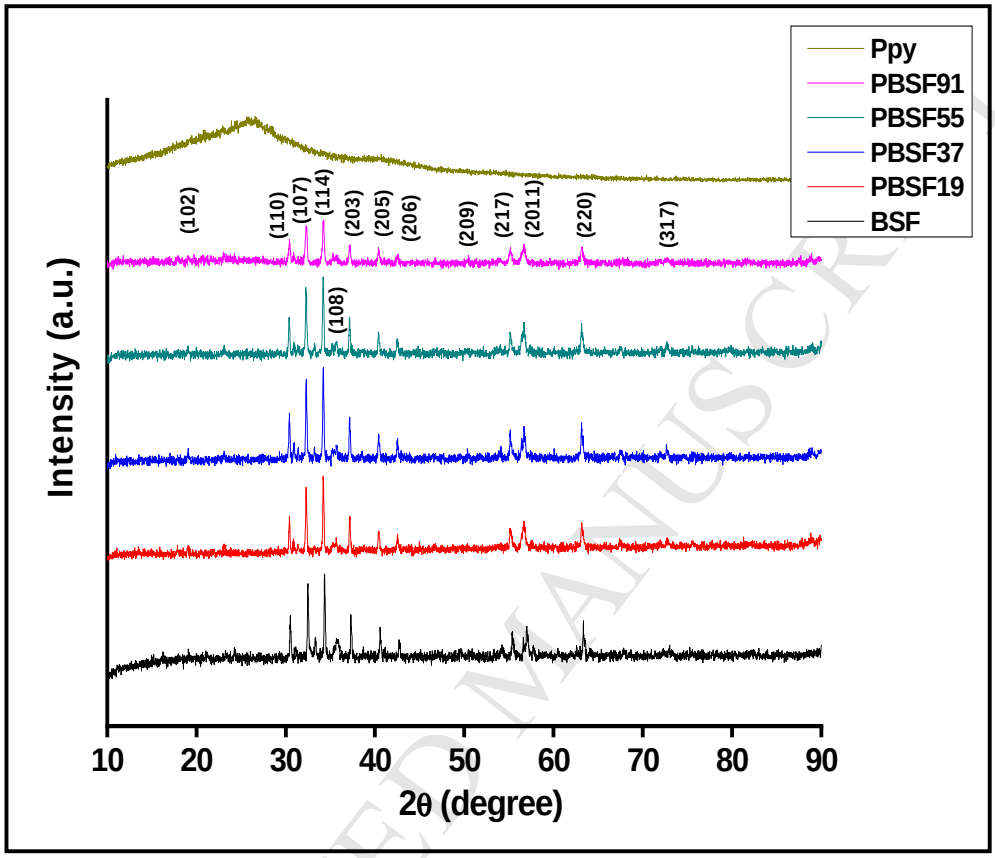

Fig. 2

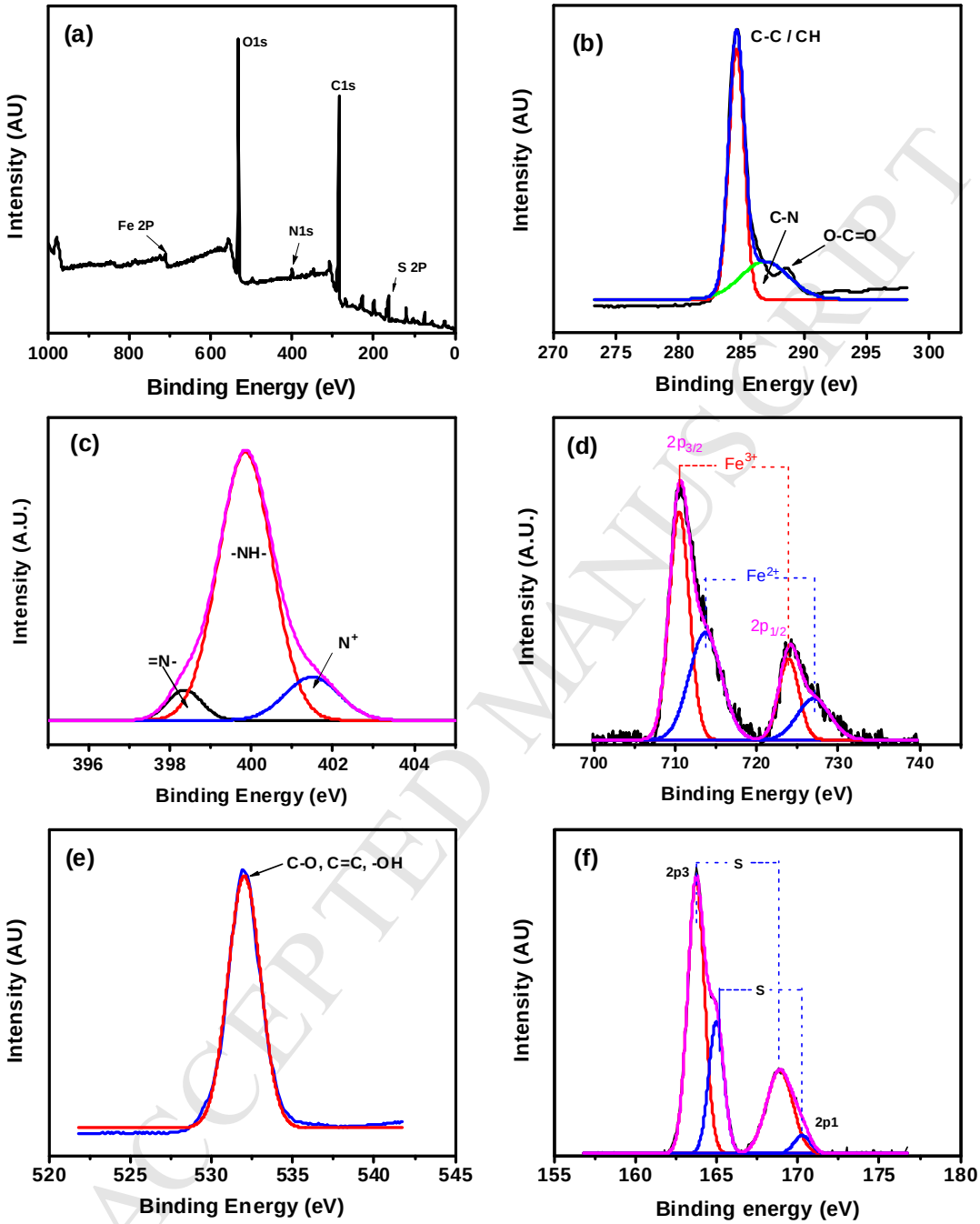

Fig. 3

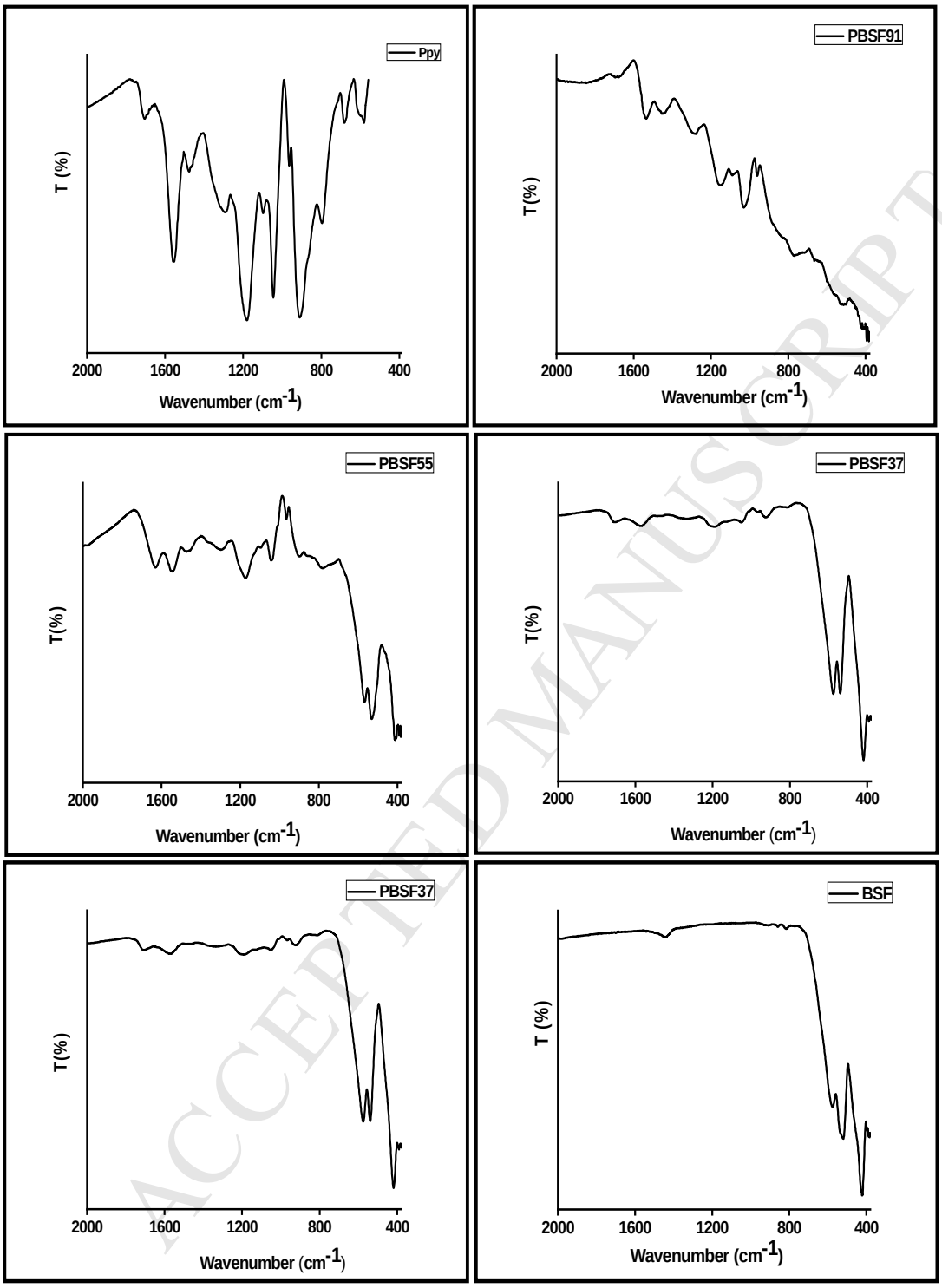

Fig. 4

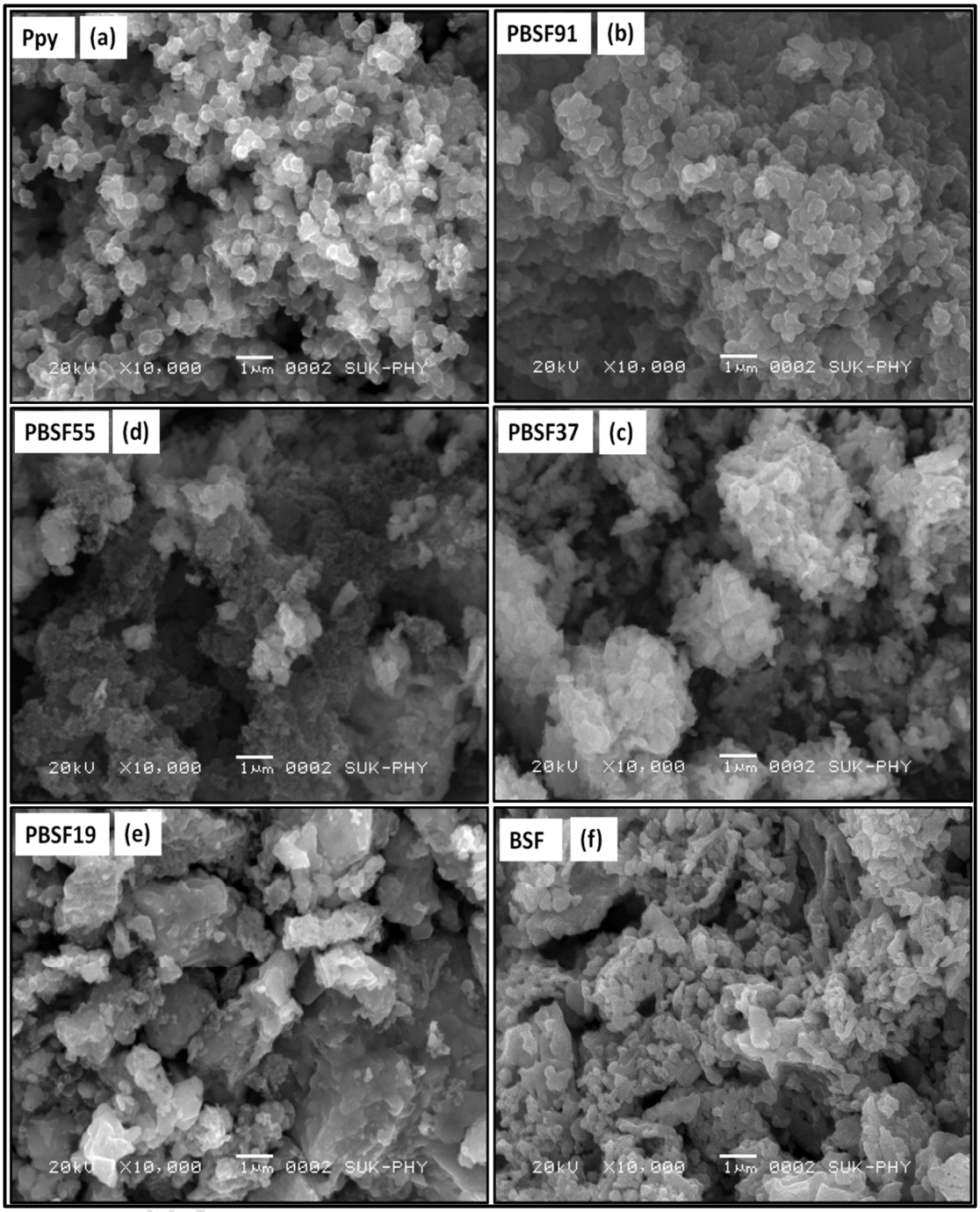
Ppy
(a)
20kV X10,000 1μm 0002 SUK-PHY
PBSF91
(b)
20kV X10,000 1μm 0002 SUK-PHY
PBSF55
(d)
20kV X10,000 1μm 0002 SUK-PHY
PBSF37
(c)
20kV X10,000 1μm 0002 SUK-PHY
PBSF19
(e)
20kV X10,000 1μm 0002 SUK-PHY
BSF
(f)
20kV X10,000 1μm 0002 SUK-PHY

Fig. 5

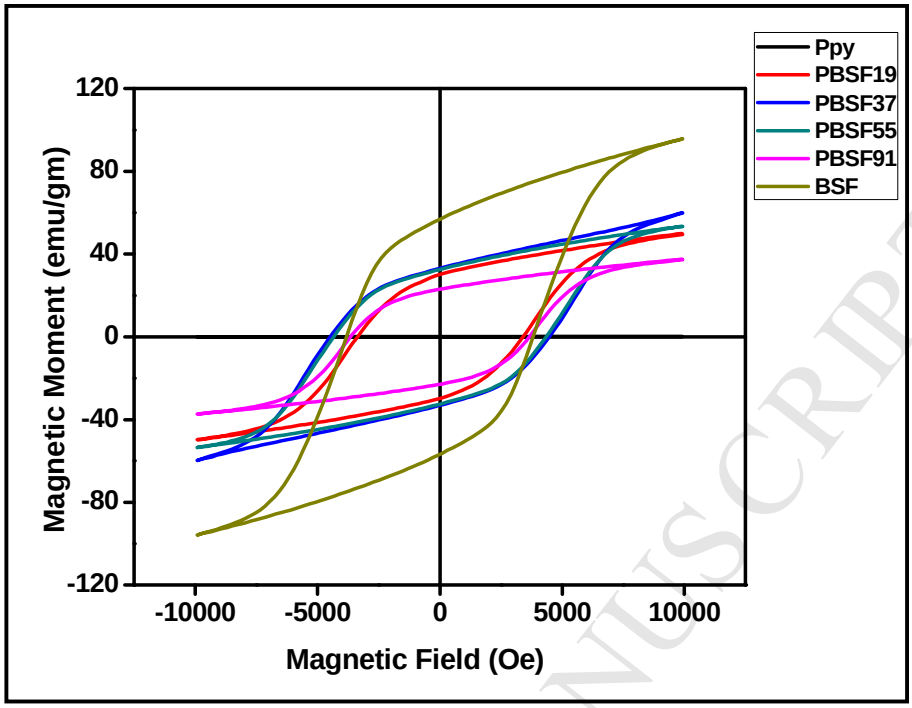

Fig. 6 (a)

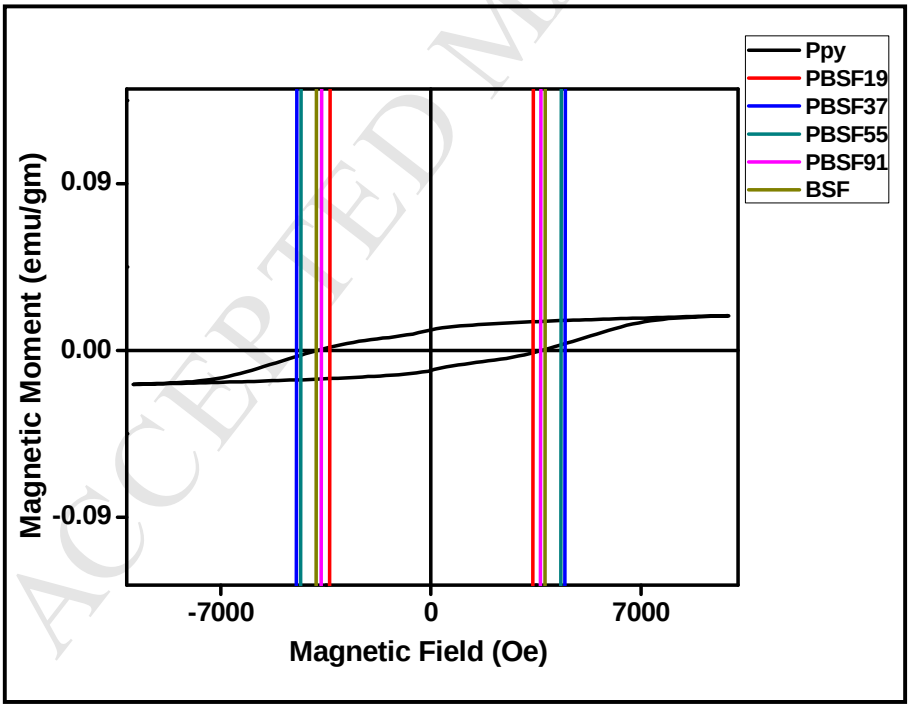

Fig. 6 (b)

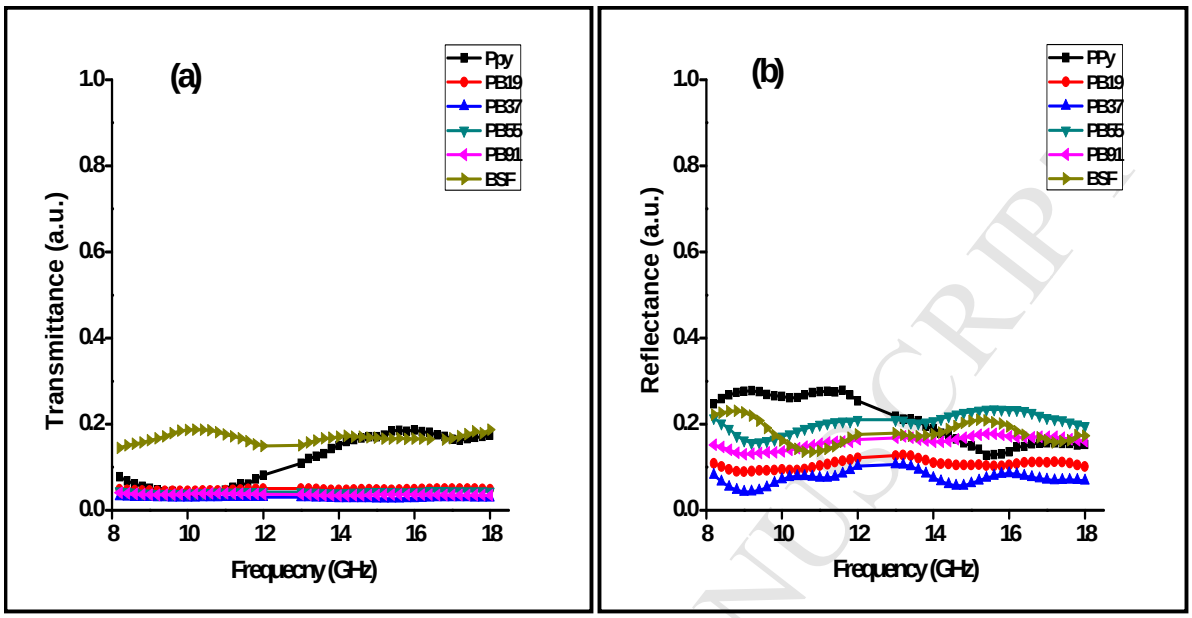

Fig. 7

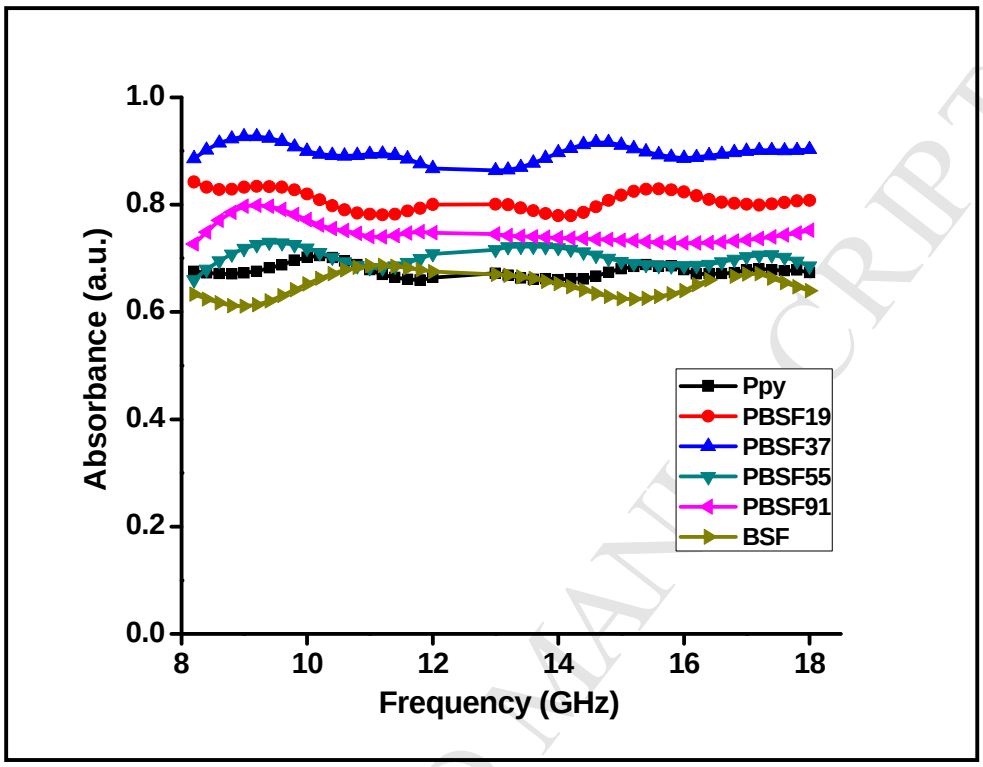

Fig. 8

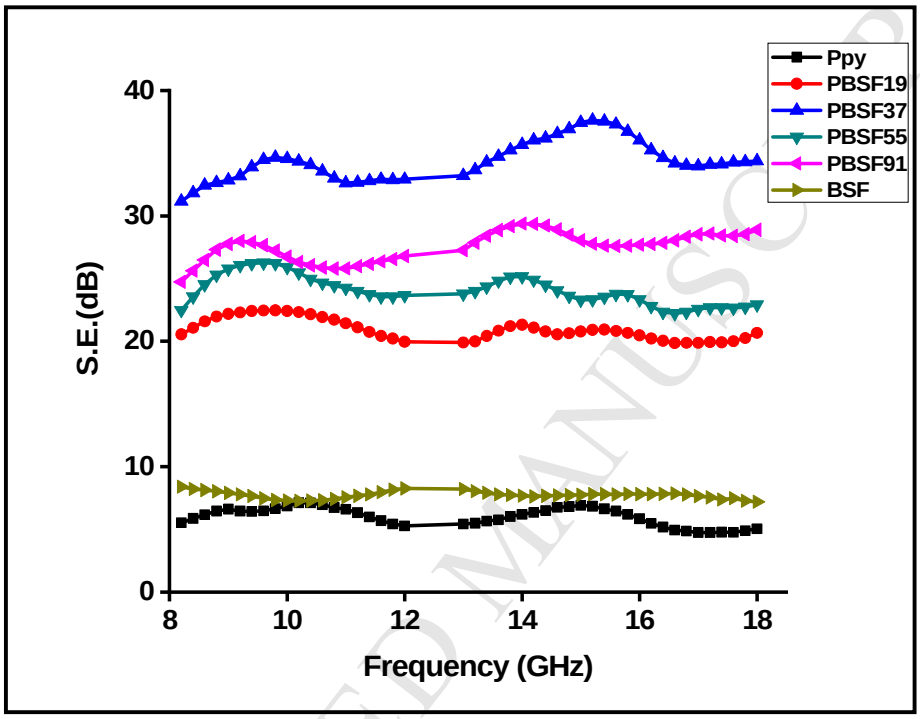

Fig. 9

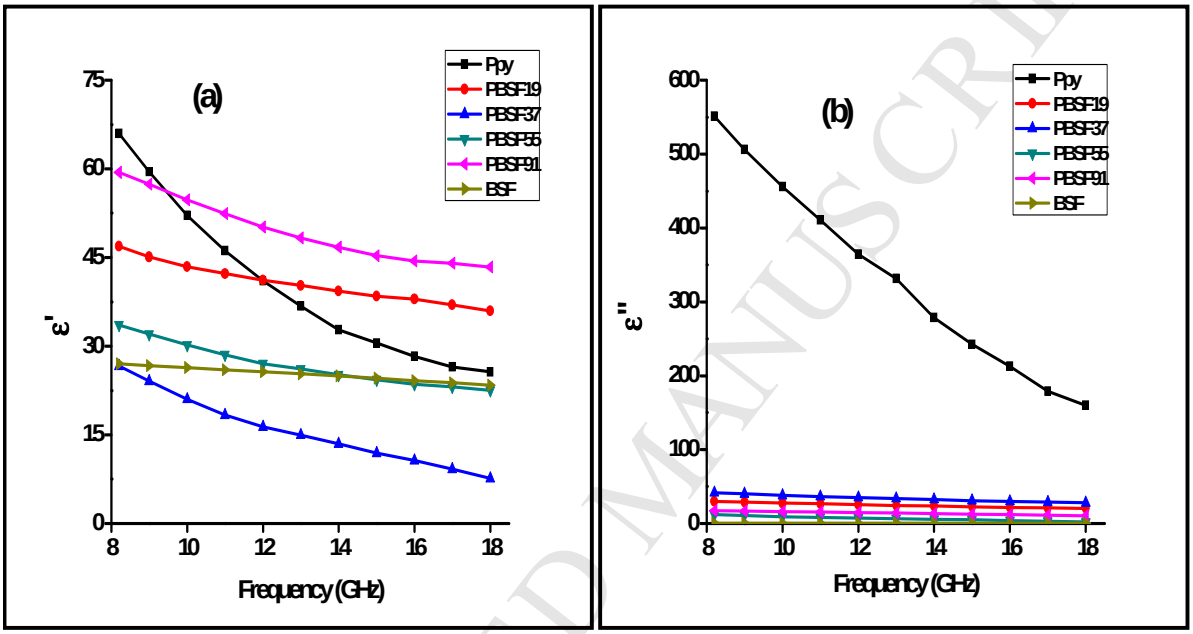

Fig. 10

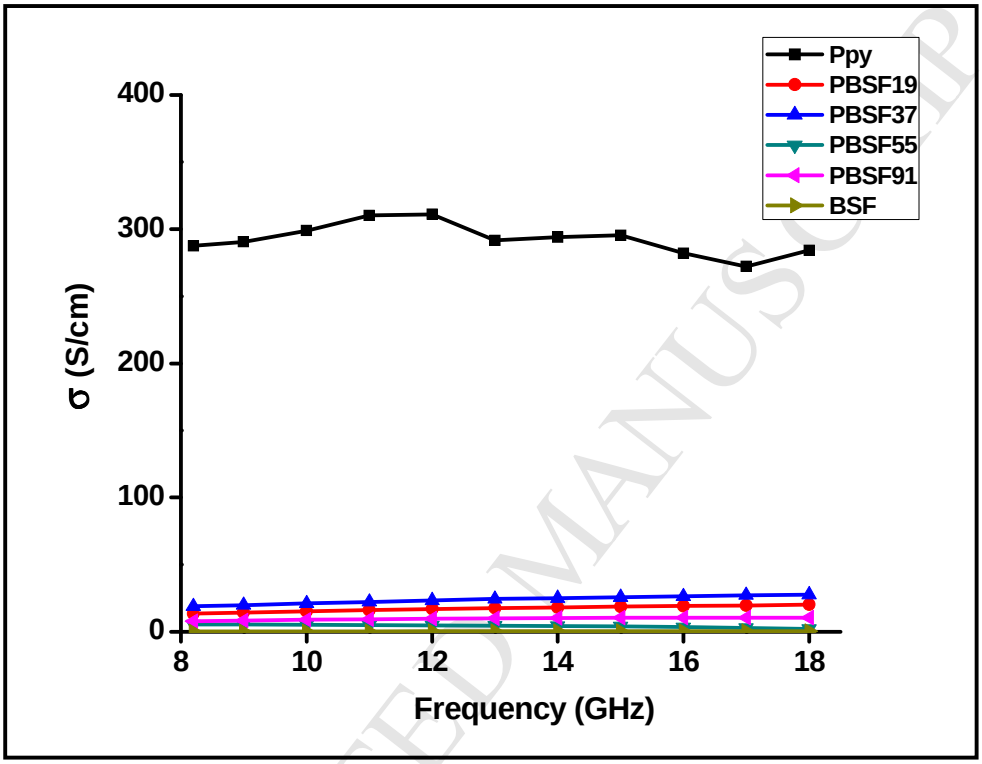

Fig. 11

Electromagnetic Shielding, Magnetic and Microwave Absorbing Properties of Polypyrrole/$Ba_{0.6}Sr_{0.4}Fe_{12}O_{19}$ Composite Synthesized *via* In-Situ Polymerization Technique

Ninad Velhal[1], N.D. Patil[1], Gopal Kulkarni[1], S. K. Shinde[2], N. J. Valekar[1], H. C. Barshilia[3], Vijaya Puri[1]*

[1]*Thick and Thin Film Device Laboratory, Department of Physics, Shivaji University, Kolhapur, 416004, India*

[2]*Department of Biological and Environmental Science, College of Life Science and Biotechnology, Dongguk University, 410-820, South Korea*

[3]*Surface engineering division, Nanomaterials Research Lab, CS-IR National Aerospace Laboratories, Kodhihalli, Bangalore, 560 017, India*

Email: vijayapuri1@gmail.com

Highlights:

- ✓ Simple and cost effective In-situ chemical polymerization technique has been used for synthesis
- ✓ First time studied the microwave properties of divalent substituted hard ferrite, polymer composite
- ✓ Maximum microwave absorption, shielding effectiveness and magnetic moment obtained for 30:70 % composition i.e. for PBSF37 sample
- ✓ The final composition can be used for the application of stealth technology as a coating for aircraft